bioRxiv preprint doi: https://doi.org/10.1101/2020.01.15.907550; this version posted January 15, 2020. The copyright holder for this preprint (which was not certified by peer review) is the author/funder. All rights reserved. No reuse allowed without permission.

Protrudin functions as a scaffold in the endoplasmic reticulum to support axon regeneration in the adult central nervous system

Veselina Petrova[1], Craig S. Pearson[2], James R. Tribble[3], Andrea G. Solano[2], Evan Reid[4], Pete A. Williams[3], Herbert M. Geller[2], Richard Eva[1,6], James W. Fawcett[1,5,6]

[1] John van Geest Centre for Brain Repair, Department of Clinical Neurosciences, University of Cambridge, UK

[2] Laboratory of Developmental Neurobiology, Division of Intramural Research, National Heart, Lung and Blood Institute, NIH, Bethesda, USA

[3] Department of Clinical Neuroscience, Division of Eye and Vision, St. Erik Eye Hospital, Karolinska Institutet, Stockholm, Sweden

[4] Cambridge Institute for Medical Research and Department of Medical Genetics, University of Cambridge, UK

[5] Centre for Reconstructive Neuroscience, Institute of Experimental Medicine AVCR, Prague, Czech Republic

[6] These authors contributed equally

Abstract:

Adult mammalian central nervous system axons have intrinsically poor regenerative capacity, so axonal injury or disease have permanent consequences. One approach to enhancing regeneration is to increase the axonal supply of growth molecules. We achieved this by expressing the adaptor molecule Protrudin which enabled robust central nervous system regeneration both *in vitro* and *in vivo* in the injured adult optic nerve. Protrudin expression facilitated the accumulation of endoplasmic reticulum and Rab11 endosomes in the distal axon, whereas removing protrudin's endoplasmic reticulum localization, kinesin-binding or phosphoinositide-binding properties abrogated the regenerative effects. These results demonstrate that Protrudin promotes regeneration by functioning as a scaffold to link axonal organelles, motors and membranes, establishing important roles for these cellular components in mediating regeneration in the adult central nervous system.

One Sentence Summary:

Protrudin promotes axon regeneration in the adult central nervous system through the mobilization of subcellular machinery.

bioRxiv preprint doi: https://doi.org/10.1101/2020.01.15.907550; this version posted January 15, 2020. The copyright holder for this preprint (which was not certified by peer review) is the author/funder. All rights reserved. No reuse allowed without permission.

Introduction

Adult central nervous system (CNS) neurons have limited ability to regenerate their axons, meaning that axonal injury or disease has life-altering consequences with little chance of recovery. Studies aimed at enhancing intrinsic regenerative capacity have identified signaling pathways, transcriptional and epigenetic programs, and the cytoskeleton as targets for promoting axon regeneration in the injured CNS (1–3). An additional target is the axonal transport of growth machinery. As CNS neurons mature and partition into somatodendritic and axonal domains, many growth-related molecules become excluded from axons, contributing to regenerative failure with maturation. Many of these growth-promoting molecules traffic through Rab11-positive recycling endosomes which are excluded from mature axons, and increasing their transport restores regenerative ability to CNS neurons maturing *in vitro* (4). In this study we focused on Protrudin, an integral endoplasmic reticulum (ER) membrane protein that facilitates the anterograde transport of Rab11 endosomes and other endosomal organelles towards neurite tips and cellular protrusions, through an interaction with kinesin 1 (KIF5) (5–7).

Results

Protrudin has several key protein domains, including a Rab11-binding domain (RBD), three hydrophobic membrane-association domains, an FFAT motif for binding to VAP proteins at ER contact sites, a coiled-coiled (CC) domain (which interacts with kinesin 1) and a phosphoinositide-binding FYVE domain (**Fig. 1A**) (5,8). Whilst Protrudin is normally targeted to the ER membrane, its atypical FYVE domain enables its interaction with other membranes including endosomes and the plasma membrane (7,9). Protrudin mRNA (*Zfyve27*) is expressed at low levels in CNS neurons, and its expression is not developmentally regulated (**Fig. S1A**) (4). In contrast, in sensory, regeneration-capable neurons, the Protrudin transcript increases with development, during axon growth *in vitro,* and in response to peripheral nerve injury (**Fig. S1B**) (10). Protrudin localizes to both axons and dendrites of developing cortical neurons but becomes enriched in dendrites when axons lose their regenerative ability with maturation (**Fig. S1C and D**). Given that Protrudin interacts with both Rab11 and kinesin 1 and is expressed at low levels in CNS neurons, we reasoned that its overexpression might increase regeneration through the axonal targeting of recycling endosomes that contain many regeneration-promoting molecules. Protrudin is regulated by phosphorylation downstream of growth factor receptor activation, leading to enhanced binding to Rab11 and protrusion formation (5). As growth factor signaling could be a limiting factor in Protrudin function in mature axons, we created a phosphomimetic, active Protrudin (3) (**Fig. 1B**). To investigate the effects of wild-type and

bioRxiv preprint doi: https://doi.org/10.1101/2020.01.15.907550; this version posted January 15, 2020. The copyright holder for this preprint (which was not certified by peer review) is the author/funder. All rights reserved. No reuse allowed without permission.

active Protrudin on axon regeneration *in vitro*, we used the laser axotomy model of regenerative decline, where axons lose their regenerative ability as they mature and become electrically active (4,11) (**Fig. 1C**). In this model, rat cortical neurons were transfected with either control (syn-mCherry), wild-type Protrudin (syn-mCherry-wild-type) or phosphomimetic active Protrudin (syn-mCherry-active) at 10 DIV, causing a substantial increase in Protrudin expression (**Fig. S2A-D**). We examined axon regeneration after laser injury at 13-17 DIV (when their regenerative capacity is low). Axons typically showed two responses to injury: 1) formation of a retraction bulb and no regeneration, or, 2) formation of a retraction bulb, followed by growth cone development and axon extension (**Fig. 1D**). Expression of either wild-type or active Protrudin led to a dramatic increase in the percentage of axons regenerating after injury (**Fig. 1E**) with axons regenerating longer distances (**Fig. 1F**) and initiating regeneration in a shorter time (**Fig. 1G**). These regenerative events were most pronounced in neurons transfected with active Protrudin. No differences in the retraction distance after injury were observed (**Fig. 1H**).

Protrudin's effect on axon regeneration was dose dependent; co-transfection with a construct encoding GFP resulted in lower Protrudin expression and a reduced effect on regeneration (**Fig. S3A-C**). Overexpressed wild-type and active Protrudin localized throughout axons, accumulating at the growth cones of uninjured axons, at regenerating growth cones, and at the retraction bulbs of non-regenerating injured axons. At the growth cone, Protrudin localized principally to the central domain (**Fig. S3D-E**). Overexpression of Protrudin had no effect on soma size, dendritic tree complexity, or spine number and morphology (**Fig. S4A-F**) whereas expression of active Protrudin during initial outgrowth (transfected at 1 DIV, measured at 4 DIV) had a modest effect on both axon and dendrite length as well as dendritic arborization length (**Fig. S4G-H**). The effect of protrudin expression is therefore specific to regeneration, with little effect on initial outgrowth.

bioRxiv preprint doi: https://doi.org/10.1101/2020.01.15.907550; this version posted January 15, 2020. The copyright holder for this preprint (which was not certified by peer review) is the author/funder. All rights reserved. No reuse allowed without permission.

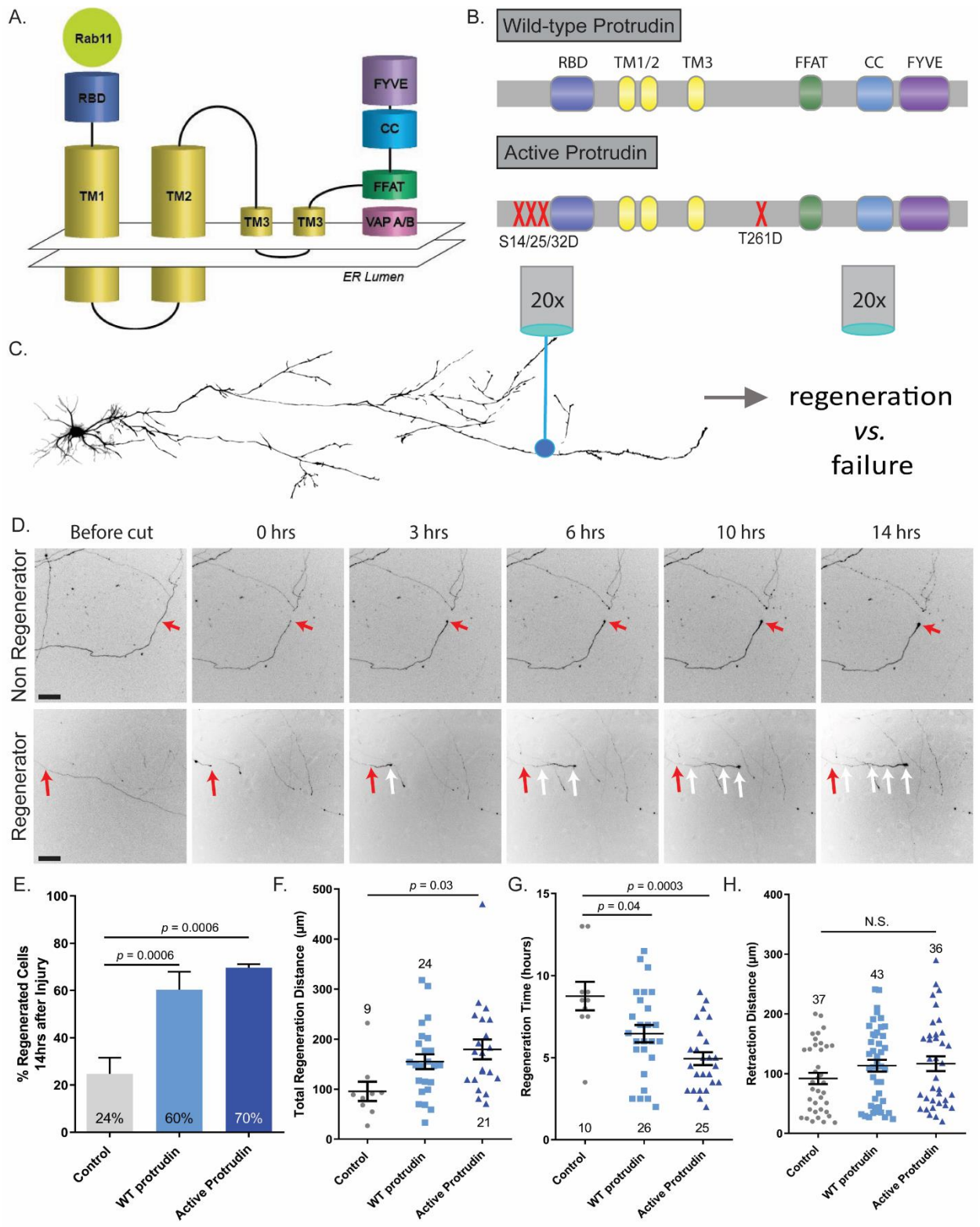

<u>Figure 1</u> Protrudin overexpression enhances axon regeneration *in vitro*. (**A**) Schematic diagram of Protrudin's domains and structure. (**B**) Schematic of wild-type and active Protrudin

bioRxiv preprint doi: https://doi.org/10.1101/2020.01.15.907550; this version posted January 15, 2020. The copyright holder for this preprint (which was not certified by peer review) is the author/funder. All rights reserved. No reuse allowed without permission.

mutagenesis sites. (**C**) Diagram of the laser axotomy method (**D**) Representative images show a regenerating and a non-regenerating axon over 14 h post laser axotomy. The red arrows at 0 h post injury shows the point of injury. The white arrows trace the path of a regenerating axon. Scale bars are 50 µm. (**E**) Percentage of regenerating axons overexpressing either mCherry control (n = 45), mCherry wild-type Protrudin (n = 45) or mCherry active Protrudin (n = 39) (*Fisher's exact* test). (**F**) Quantification of regeneration distance 14 h after injury (*One-way ANOVA*, p = 0.04). (**G**) Quantification of regeneration initiation time (*One-way ANOVA*, p = 0.0004). (**H**) Quantification of retraction distance (*One-way ANOVA*, p = 0.214). Error bars represent mean ± SEM.

During axonal maturation, Rab11 endosomes and some of their cargo such as integrin alpha 9 (α9), become excluded from CNS axons, and restoring their axonal levels enhances regeneration *in vitro* (4,12). To determine whether Protrudin's regenerative effects were accompanied by an increase in the axonal transport of integrins and Rab11 endosomes, we used spinning-disc live-cell microscopy to observe the movement of Rab11-GFP or integrin α9-GFP in the distal part of the axon in the presence of overexpressed wild-type or active Protrudin (**Fig. 2A**). Vesicle transport was scored as anterograde, retrograde, bidirectional or static and the total number of Rab11 or integrin α9-positive endosomes per section of axon was measured. The majority of Rab11-positive vesicles trafficked bidirectionally whereas the bulk of integrin-containing endosomes moved retrogradely confirming previous studies (11,13). Overexpression of wild-type or active Protrudin resulted in increased retrograde and bidirectional transport of Rab11-GFP and enhanced anterograde and retrograde transport of integrin α9-GFP (**Fig. 2B-D**), leading to more total Rab11 and integrin-positive vesicles in the distal axon (**Fig. 2B-D**). Approximately 20% of α9-transporting vesicles were positive for Protrudin (**Fig. S5**) and 29% of Protrudin-positive endosomes (wild-type or active) were also Rab11-positive (**Fig. S5**), and kymograph analysis demonstrated dynamic co-localization of both Rab11 and α9-integrin with Protrudin.

This study focused on integrin α9 because of its ability to promote long-range axon regeneration in the spinal cord (14); however, the effects of protrudin on axon growth are most likely both integrin dependent and independent (13). In addition to integrins, Rab11 endosomes transport many growth-promoting molecules that could influence regeneration including the IGF-1 and

bioRxiv preprint doi: https://doi.org/10.1101/2020.01.15.907550; this version posted January 15, 2020. The copyright holder for this preprint (which was not certified by peer review) is the author/funder. All rights reserved. No reuse allowed without permission.

TrkB receptors (15,16). Rab11 may also promote regeneration through regulation of membrane trafficking events (17).

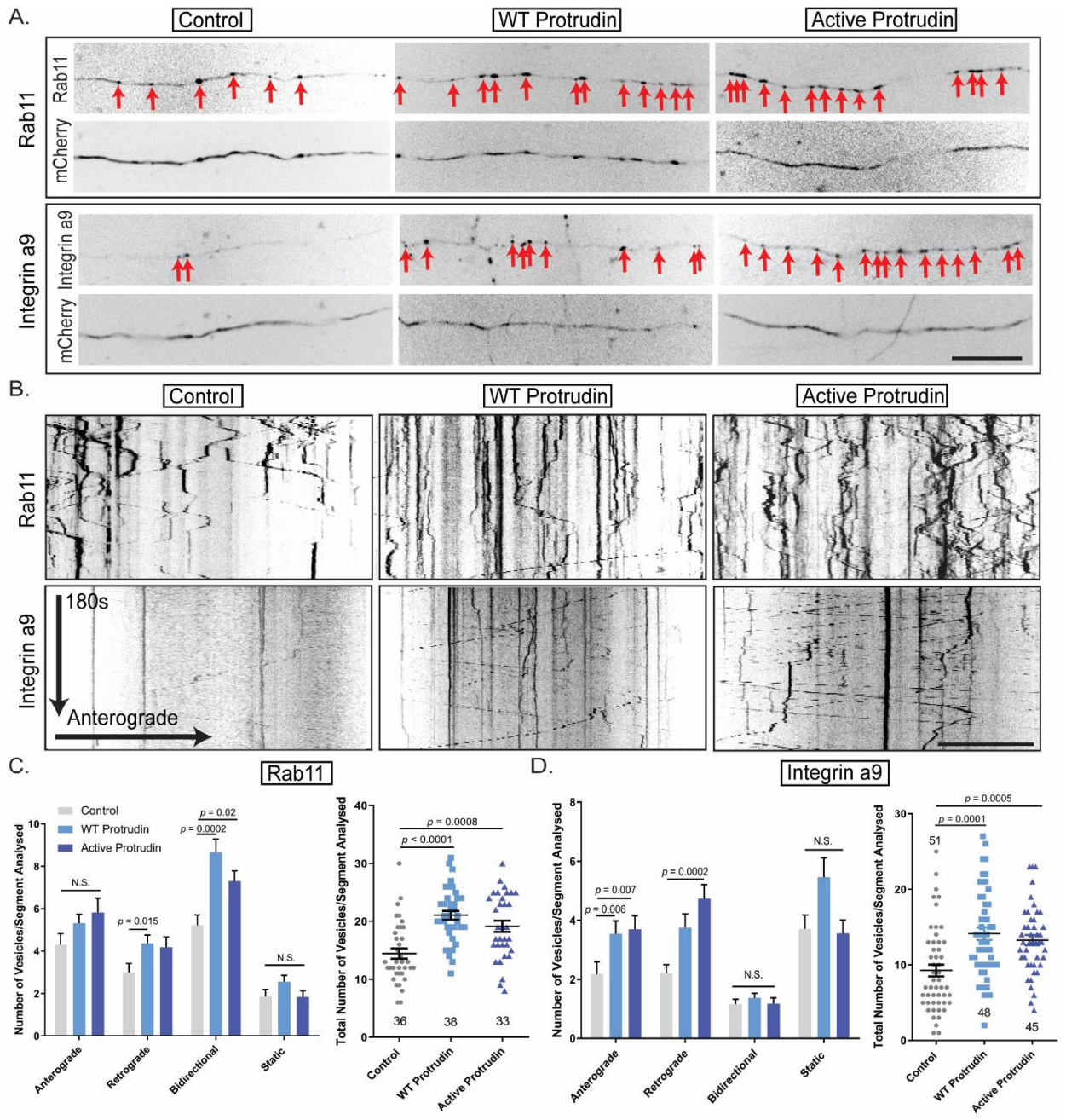

<u>Figure 2</u> Protrudin enhances the transport of growth machinery and receptors in the distal axon. (**A**) Representative distal axon sections of neurons expressing integrin α9-GFP or Rab11-GFP, together with either mCherry (control), mCherry-wild-type Protrudin or mCherry-active Protrudin. (**B**) Kymographs showing the dynamics of integrin α9-GFP and Rab11-GFP in distal

bioRxiv preprint doi: https://doi.org/10.1101/2020.01.15.907550; this version posted January 15, 2020. The copyright holder for this preprint (which was not certified by peer review) is the author/funder. All rights reserved. No reuse allowed without permission.

axons of co-transfected neurons. Scale bar is 10 µm. (**C**) Quantification of Rab11-GFP axon vesicle dynamics and total number of Rab11 GFP vesicles in distal axon sections (*Kruskal-Wallis with Dunn's* multiple comparison test) (**D**) Quantification of integrin α9-GFP axon vesicle dynamics and total number of integrin α9-GFP vesicles in distal axon sections (*Kruskal-Wallis with Dunn's* multiple comparison test). Error bars represent mean ± SEM.

To test the contribution of Protrudin's key domains to its regenerative effects, we assembled a cohort of mutants in accordance with previous literature (5,6,8,9,18), targeting the FYVE domain, FFAT domain, Rab11-binding domain (RBD), and KIF5-interacting domain, as well as a mutant lacking all three transmembrane (TM) domains (**Fig. 3A**). Deletion of these hydrophobic regions releases Protrudin from the ER membrane, rendering it cytosolic (8). Each of these mutants was separately expressed in primary rat cortical neurons at 10 DIV and their effects on axon regeneration were studied at 13-17 DIV using laser axotomy. Overexpression of the RBD mutant caused neuronal cell death (**Fig. S5C**), indicating an essential role for the Protrudin-Rab11 interaction in neuronal viability but precluding examination of its effect on axon regeneration. All other mutants sharply diminished the effects of Protrudin overexpression on axon regeneration, whilst active Protrudin again stimulated robust regeneration (**Fig. 3B**). This demonstrates that each domain is required for, and contributes equally to enhancing axon regrowth after injury.

The finding that the FFAT mutant and the TM1-3 mutant suppressed Protrudin-induced regeneration demonstrates that ER localization is essential for Protrudin's regenerative effects, indicating an important role for the ER in mediating CNS axon regeneration. The ER exists as a continuous tubular organelle through axons (similar to an axon within the axon), and its genetic disruption causes axonal degeneration (19). Re-establishment of the axonal ER may be equally as important as the re-establishment of the axon membrane for successful regeneration. Because ER tubules undergo highly dynamic movements, partly by hitchhiking on motile endosomes (20), we hypothesized that increased axonal transport caused by Protrudin overexpression might be accompanied by an increase in tubular ER in the axon. To examine the effects of Protrudin overexpression on axonal ER we analyzed the distribution of reticulon 4, which reliably reports on ER abundance in axons (21) (**Fig. 3C**). Overexpression of wild-type and active Protrudin resulted in increased reticulon 4 in the growth cone shaft and at the axon tip of uninjured axons

bioRxiv preprint doi: https://doi.org/10.1101/2020.01.15.907550; this version posted January 15, 2020. The copyright holder for this preprint (which was not certified by peer review) is the author/funder. All rights reserved. No reuse allowed without permission.

(**Fig. 3D-E**). Crucially, mutation of FFAT or TM1-3 domains abolished this effect. Collectively, these results demonstrate that Protrudin enables axon regeneration by acting as a scaffold within the distal axonal ER, linking recycling endosomes, kinesin 1, and phosphoinositides, and enabling transport of ER and endosomes to regenerating growth cones.

There are several mechanisms by which ER could facilitate axon regeneration, including bulk transfer of lipids from the ER to the plasma membrane, synthesis and transfer of signaling lipids, and calcium signaling. Protrudin-mediated enrichment of ER into the tip of growing or injured processes could function to enable the transfer of lipids, with the FYVE domain permitting interaction with the surface membrane (9), allowing for rapid expansion of the growth cone plasma membrane - a requirement for successful axon regeneration (22).

bioRxiv preprint doi: https://doi.org/10.1101/2020.01.15.907550; this version posted January 15, 2020. The copyright holder for this preprint (which was not certified by peer review) is the author/funder. All rights reserved. No reuse allowed without permission.

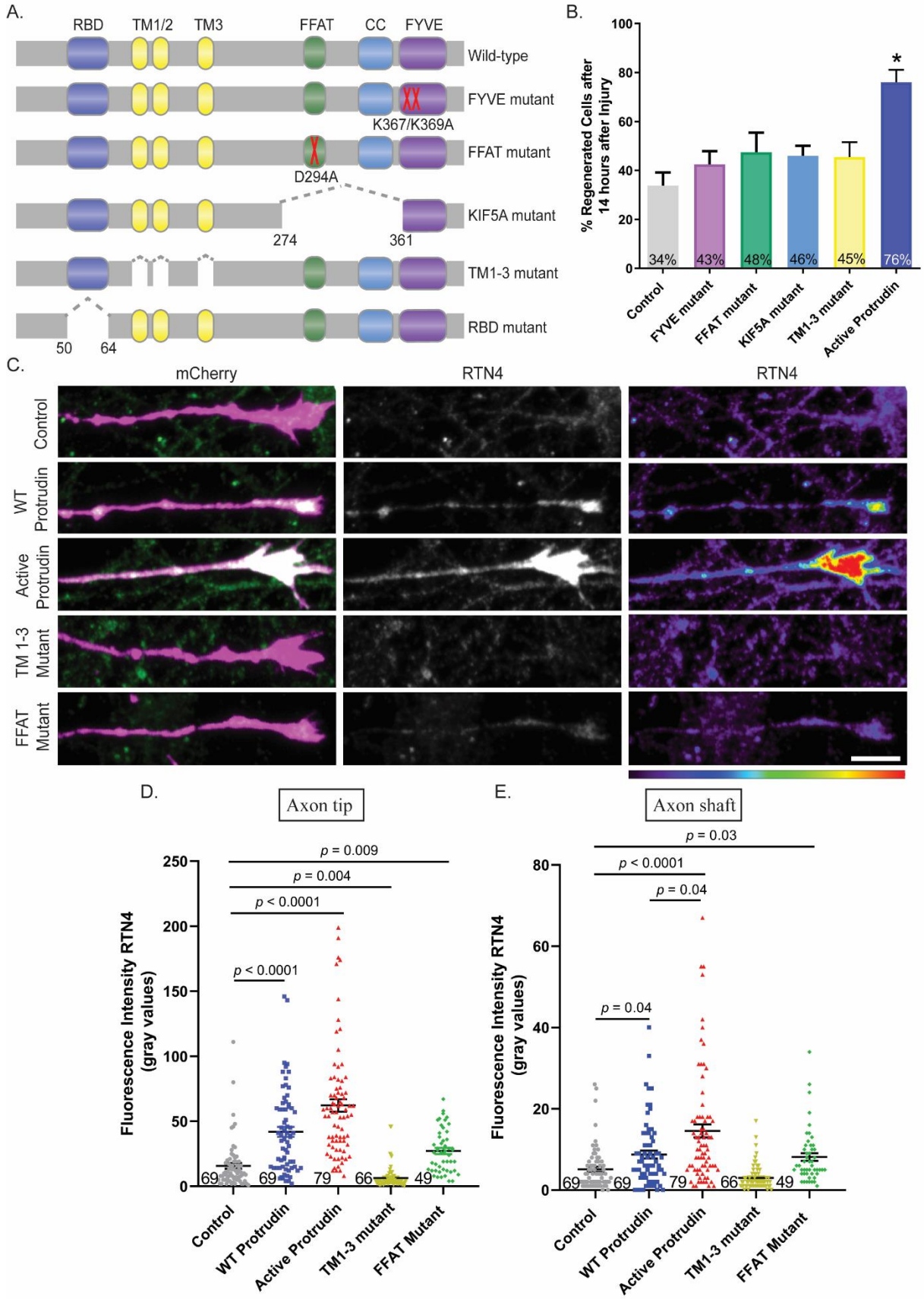

bioRxiv preprint doi: https://doi.org/10.1101/2020.01.15.907550; this version posted January 15, 2020. The copyright holder for this preprint (which was not certified by peer review) is the author/funder. All rights reserved. No reuse allowed without permission.

Figure 3 Protrudin overexpression enhances axon regeneration through multiple mechanisms. (**A**) Schematic representation of Protrudin domain mutants. (**B**) Percentage of regenerating axons in neurons expressing mCherry-Protrudin domain mutants – FYVE (n = 56), FFAT (n = 60), KIF5A (n = 56), TM1-3 (n = 45) compared active Protrudin as a positive control (n = 42), and mCherry as a negative control (n = 83). (**C**) Representative images of RTN4 immunofluorescence (green) in the distal axon of neurons expressing the indicated m-Cherry Protrudin constructs (magenta). Scale bar is 10 µm. (**D-E**) Quantification of RTN4 fluorescence intensity at the axon tip and shaft ($p < 0.0001$, *Kruskal-Wallis with Dunn's* multiple comparisons test). Error bars represent mean ± SEM.

Protrudin's robust effect on CNS axon regeneration *in vitro* prompted us to investigate its effectiveness on optic nerve regeneration. Promoting retinal ganglion cell (RGC) regeneration has the potential to restore vision loss associated with optic neuropathies such as glaucoma, and virally-delivered gene therapy for eye disease is already in clinical practice (23). We first examined Protrudin mRNA levels in RGCs in published RNAseq datasets (24) and found that Protrudin mRNA is present at low levels in mature, adult RGCs (**Fig. S6A**). This corresponded with our findings for cortical neurons but not regenerative PNS neurons (**Fig. S1A-B**). We generated three constructs for AAV delivery to the retina by intravitreal injection: AAV2-GFP, AAV2-Protrudin-GFP, and AAV2-activeProtrudin-GFP. The viruses transduced 40-45% of retinal ganglion cells (RGCs) throughout the retina (**Fig. S6B-E**). Viruses were injected 2 weeks before optic nerve crush, and 2 weeks after injury the anterograde axon tracer – cholera toxin subunit-ß (CTB) was administered (**Fig. 4A**). Control optic nerves had limited regeneration (0% >0.5 mm from the crush site), while regenerating axons extended to 2.75 mm for wild-type Protrudin-transduced animals, and 3.5 mm for active Protrudin-transduced animals. The numbers of regenerating axons were high, particularly for active Protrudin, in which over 630 axons were seen proximally, significantly more than in control (44 axons) or in wild-type Protrudin (380 axons) (**Fig. 4B-C**). Co-localization between CTB and GAP43 was found throughout the nerve in all conditions suggesting that the majority of CTB-positive axons observed in the nerve past the injury site are regenerating axons (**Fig. S6F**). We also examined the effects of Protrudin expression on RGC survival. Because optic nerve injury leads to severe neuronal loss two weeks after injury (typically 80-90%) we used an acute retinal explant model which is often used to detect potential neuroprotective treatments for

bioRxiv preprint doi: https://doi.org/10.1101/2020.01.15.907550; this version posted January 15, 2020. The copyright holder for this preprint (which was not certified by peer review) is the author/funder. All rights reserved. No reuse allowed without permission.

glaucoma (24–26). Viruses were injected intravitreally, and retinas were removed two weeks later and cultured as explants for three days. Both wild-type and active Protrudin were entirely neuroprotective, with these retinas exhibiting no loss of RGC neurons, whilst GFP-only controls lost 55% of their RGCs (**Fig. 4D-F**).

Our study demonstrates robust axon regeneration in the adult CNS driven by overexpression of the adapter protein Protrudin. Overexpression of Protrudin, particularly in its phosphomimetic, active form allows long-range regeneration in cortical neurons and in the injured adult optic nerve. Importantly, both Protrudin and active Protrudin expression lead to an accumulation of ER in the distal axon and interfering with Protrudin's ER localization domains abrogates its regenerative effects, indicating a central role for the ER in mediating Protrudin-driven regeneration. We propose that Protrudin enables regeneration by acting as a scaffold to link the ER, recycling endosomes, kinesin-based transport and membrane phospholipids. Our findings establish the importance of these components in facilitating CNS axon regeneration, whilst suggesting Protrudin gene-therapy as a potential approach for repairing CNS axon damage.

bioRxiv preprint doi: https://doi.org/10.1101/2020.01.15.907550; this version posted January 15, 2020. The copyright holder for this preprint (which was not certified by peer review) is the author/funder. All rights reserved. No reuse allowed without permission.

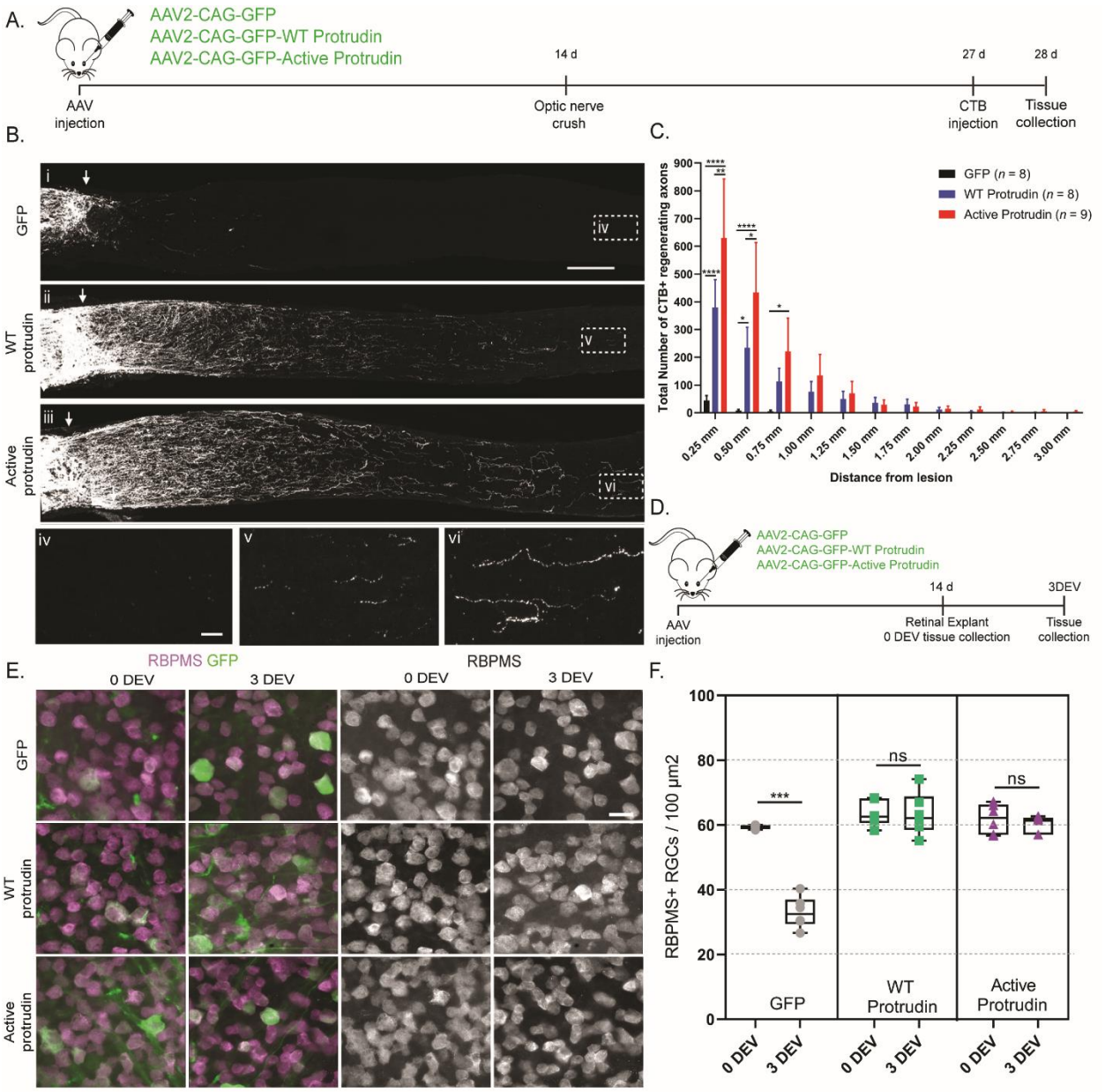

<u>Figure 4</u> Protrudin enhances regeneration and survival of RGC axons. (**A**) Experiment timeline for optic nerve crush. (**B**) CTB-labelled axons in the optic nerves of mice transduced with viruses for wildtype (WT) Protrudin, active Protrudin and GFP control. Arrows indicate lesion site. Insets (iv-vi) show regenerating axons in the distal optic nerve. Scale bar is 200 µm and on inset is 20 µm (n = 8-9 animals/group). (**C**) Quantification of regenerating axons at increasing distances distal to the lesion site, displayed as mean ± SEM. Statistical significance was determined by *two-way ANOVA with Bonferroni post-hoc* test for multiple comparisons. ** $p < 0.005$, *** $p < 0.001$, **** $p < 0.0001$ (**D**) Experimental timeline for retinal explant experiment. (**E**)

bioRxiv preprint doi: https://doi.org/10.1101/2020.01.15.907550; this version posted January 15, 2020. The copyright holder for this preprint (which was not certified by peer review) is the author/funder. All rights reserved. No reuse allowed without permission.

Representative images of RGCs (magenta for RBPMS) 0 and 3 days *ex vivo* (DEV) in eyes injected with each virus. (**F**) Quantification of RGC survival in retinal explant (*Student's* t-test). ** $p < 0.005$, *** $p < 0.001$, **** $p < 0.0001$.

1. Z. He, Y. Jin, Intrinsic control of axon regeneration. *Neuron*, **90(3)**, 437–51 (2016).

2. A. Tedeschi, F. Bradke, Spatial and temporal arrangement of neuronal intrinsic and extrinsic mechanisms controlling axon regeneration. *Curr Opin Neurobiol*, **42**, 118–127 (2017).

3. V. Petrova, R. Eva, The virtuous cycle of axon growth: Axonal transport of growth-promoting machinery as an intrinsic determinant of axon regeneration. *Dev. Neurobiol.* **78(10)**, 898-925 (2018).

4. H. Koseki et al., Selective rab11 transport and the intrinsic regenerative ability of CNS axons. *eLife*, **6**: e26596 (2017).

5. M. Shirane, K. Nakayama, Protrudin induces neurite formation by directional membrane trafficking. *Science*, **314(5800)**, 818–821 (2006).

6. F. Matsuzaki et al., Protrudin serves as an adaptor molecule that connects KIF5 and its cargoes in vesicular transport during process formation. *Mol. Biol. Cell*, **22(23)**, 4602–4620 (2011).

7. C. Raiborg et al., Repeated ER–endosome contacts promote endosome translocation and neurite outgrowth. *Nature*, **520(7546)**, 234–238 (2015).

8. J. Chang et al., Protrudin binds atlastins and endoplasmic reticulum-shaping proteins and regulates network formation. *Proc. Natl. Acad. Sci.* **110(37)**, 14954–14959 (2013).

9. J.E. Gil et al., Phosphoinositides differentially regulate protrudin localization through the FYVE domain. *J. Biol. Chem.* **287(49)**, 41268–41276 (2012).

10. A. Tedeschi et al., The calcium channel subunit Alpha2delta2 suppresses axon regeneration in the adult CNS. *Neuron*, **92(2)**: 419–434 (2016).

11. R. Eva et al. EFA6 regulates selective polarised transport and axon regeneration from the

bioRxiv preprint doi: https://doi.org/10.1101/2020.01.15.907550; this version posted January 15, 2020. The copyright holder for this preprint (which was not certified by peer review) is the author/funder. All rights reserved. No reuse allowed without permission.

axon initial segment. *J. Cell Sci.*, **130(21)**,3663–3675 (2017).

12. M.R. Andrews et al., Axonal localization of integrins in the CNS is neuronal type and age dependent. *eNeuro* **3(4)**, ENEURO.0029-16.2016 (2016).

13. R. Eva et al., Rab11 and its effector Rab coupling protein contribute to the trafficking of integrins during axon growth in adult dorsal root ganglion neurons and PC12 cells. *J. Neurosci.* **30(35)**, 11654–11669 (2010).

14. M.R. Andrews et al. Alpha9 integrin promotes neurite outgrowth on tenascin-C and enhances sensory axon regeneration. *J. Neurosci.* **29(17)**, 5546–57 (2009).

15. R. Romanelli et al., Insulin-like growth factor type-I receptor internalization and recycling mediate the sustained phosphorylation of Akt. *J. Biol. Chem.* **282(31)**, 22513–22524 (2007).

16. E. Hollis et al., Induction of corticospinal regeneration by lentiviral trkB-induced Erk activation. *Proc. Natl. Acad. Sci.* **106(17)**, 7215–7220 (2009).

17. C. Campa, E. Hirsch, Rab11 and phosphoinositides: A synergy of signal transducers in the control of vesicular trafficking. *Adv. Biol. Regul.* **63**, 132–139.

18. S. Saita et al., Promotion of neurite extension by protrudin requires its interaction with vesicle-associated membrane protein-associated protein. *J. Biol. Chem.* **284(20)**, 13766–13777 (2009).

19. B. Yalçın et al. Modeling of axonal endoplasmic reticulum network by spastic paraplegia proteins. *eLife*, **6,** e23882 (2017).

20. Y. Guo et al., Visualizing intracellular organelle and cytoskeletal interactions at nanoscale resolution on millisecond timescales. *Cell* **175(5)**, 1430-1442 (2018).

21. G.G. Farías et al. Feedback-Driven Mechanisms between Microtubules and the Endoplasmic Reticulum Instruct Neuronal Polarity. *Neuron*, **102(1),** 184-201 (2019).

22. F. Bradke et al., Assembly of a new growth cone after axotomy: the precursor to axon regeneration. *Nat. Rev. Neurosci.* **13(3)**, 183–193 (2012).

23. J.W.B Bainbridge et al., Effect of gene therapy on visual function in Leber's congenital

bioRxiv preprint doi: https://doi.org/10.1101/2020.01.15.907550; this version posted January 15, 2020. The copyright holder for this preprint (which was not certified by peer review) is the author/funder. All rights reserved. No reuse allowed without permission.

amaurosis. *N. Engl. J. Med*. **358(21)**, 2231–2239 (2008).

24. P.A.Williams et al. Vitamin B3 modulates mitochondrial vulnerability and prevents glaucoma in aged mice. *Science*, **355(6326)**, 756–760 (2017).

25. N.D. Bull et al., Use of an adult rat retinal explant model for screening of potential retinal ganglion cell neuroprotective therapies. *Investig. Ophthalmol. Vis. Sci*., **52(6)**, 3309–3320 (2011).

26. U. Pattamatta et al., A mouse retinal explant model for use in studying neuroprotection in glaucoma. *Exp. Eye Res.* **151**, 38–44 (2016).

27. J.W. Connell et al., ESCRT-III-associated proteins and spastin inhibit protrudin-dependent polarised membrane traffic. *Cell. Mol. Life Sci*. https://doi.org/10.1007/s00018-019-03313-z (2019).

28. C.S. Pearson et al., Identification of a critical sulfation in chondroitin that inhibits axonal regeneration. *eLife*, **7,** e37139 (2018).

bioRxiv preprint doi: https://doi.org/10.1101/2020.01.15.907550; this version posted January 15, 2020. The copyright holder for this preprint (which was not certified by peer review) is the author/funder. All rights reserved. No reuse allowed without permission.

Acknowledgments:

We would like to thank Prof. Joost Verhaagen for providing the viral constructs in which Protrudin was cloned, Dr Andrew Osborne for supervising during eye injections, animal perfusions and tissue collections when validating the efficacy of the Protrudin viruses, Mr Tolga Sadku for creating the Protrudin schematic diagram, the Light Microscopy Core of the NHLBI/NIH, and Mr. Raymond Fields at the National Institute of Neurological Diseases and Stroke Viral Core Facility for making the Protrudin viruses.

Funding:

Funding was from the UK Medical Research Council; Christopher and Dana Reeve Foundation; EU ERANET Neurone; Bill and Melinda Gates Foundation; International Foundation for Research in Paraplegia (IRP); Vetenskapsrådet 2018-02124 (PAW); Pete Williams is supported by the Karolinska Institutet in the form of a Board of Research Faculty Funded Career Position and by St. Erik Eye Hospital philanthropic donations. Initial Protrudin constructs were made in Dr E. Reid's laboratory under the Wellcome Trust Senior Research Fellowship grant (082381); Division of Intramural Research, National Heart, Lung, and Blood Institute, NIH.

Author contributions:

Conceptualization, V.P., R.E., E.R. J.W.F.; Methodology, V.P., R.E., C.S.P., J.R.T, P.A.W., J.W.F.; Validation, V.P., C.S.P., A.S., J.R.T; Formal Analysis, V.P., C.S.P., A.S., J.R.T.; Investigation, V.P., C.S.P., A.S., J.R.T.; Data Curation, V.P., R.E., C.S.P., J.R.T., P.A.W.; Writing – Original Draft, V.P., R.E., J.W.F.; Writing – Review and Editing, all; Visualization, V.P., R.E., C.S.P., J.R.T., P.A.W; Supervision, E.R., P.A.W., H.M.G., R.E., J.W.F.; Funding Acquisition, V.P, P.A.W., H.M.G., R.E., J.W.F.

Competing interests: Authors declared no competing interests.

bioRxiv preprint doi: https://doi.org/10.1101/2020.01.15.907550; this version posted January 15, 2020. The copyright holder for this preprint (which was not certified by peer review) is the author/funder. All rights reserved. No reuse allowed without permission.

Supplementary Materials

Materials and Methods

DNA constructs

Human Protrudin constructs (in pmCherry-C1 and pEGFP-C1) (27), CMV-integrin-alpha9-GFP (8) and CMV-Rab11 -GFP (4,8) were used. The CMV promoter in all constructs was replaced by a human synapsin (Syn) promoter by Gibson assembly cloning. The viral vector plasmid backbones (AAV2-sCAG-GFP) were a kind donation by Prof. Joost Verhaagen, The Netherlands Institute for Neuroscience. Protrudin-GFP was cloned from pEGFP-C1 plasmid into viral vector plasmids using Gibson cloning. Site-direct mutagenesis was performed in order to create the Protrudin active phosphomimetic form (QuikChange II Site-Directed Mutagenesis Kit, Agilent Technologies). All constructs were verified by DNA sequencing.

Cell culture and transfections

Rat cortical neurons were dissected from E18 embryos and plated on imaging dishes or on acid-washed glass coverslips at the following densities: $1x10^5$cells/dish for immunocytochemistry, $2x10^5$ for axotomy or live-cell imaging and $8x10^4$ cells/coverslip. All surfaces were coated with poly-D-lysine, diluted in borate buffer to a final concentration 50 µg/mL. The cells were grown in serum-free MACS Neurobasal Media supplemented with 2% NeuroBrew21 and 1% GlutaMAX supplements at 37°C in 7% CO2 incubator. Cortical neurons were transfected using NeuroMag magnetofection system where 7µg of DNA plasmid is mixed with 100µL NB media and 8µL of magnetic beads. The reaction was kept for 30 minutes at 37°C before adding 900µL of pre-warmed NB media to a final volume of 1 mL. The original neuronal media was removed, and 1 mL of transfection mixture was added. Dishes were then incubated at 37°C for 30 minutes on a magnetic plate before the original media was returned on the plates. Plasmid reporter gene expression was observed 48 hours post-transfection.

Immunostaining

Cortical neurons were fixed in 3% PFA for 15 minutes and then thoroughly washed and kept in PBS at 4°C. Cells were permeabilized in 3% BSA in PBS and 0.1% Triton for 5 minutes and then

bioRxiv preprint doi: https://doi.org/10.1101/2020.01.15.907550; this version posted January 15, 2020. The copyright holder for this preprint (which was not certified by peer review) is the author/funder. All rights reserved. No reuse allowed without permission.

blocking solution was added (3% BSA in PBS) for 1 hour at room temperature. Primary antibodies were added at the correct concentration and kept for 1.5 hours at room temperature. Antibodies were then washed 3 times in PBS for 5 minutes. Secondary antibodies were applied at the correct concentration for 1 hour at room temperature in a dark chamber. The cells were then washed three times in 1xPBS and mounted using coverslips and Diamond anti-fade mounting agent with DAPI (Molecular Probes) or FluorSave mounting reagent (Calbiochem). Mice were anesthetized using 1-2% isoflurane and transcardially perfused with PBS followed by 4% paraformaldehyde (PFA). Optic nerves were dissected and immersed in 4% PFA. The tissue was post-fixed overnight, then immersed in 30% sucrose for 24 h for cryoprotection. Tissue was embedded in Tissue-Tek OCT and snap-frozen for cryosectioning. 14 μm-thick longitudinal sections of the optic nerve were obtained on charged Superfrost microscope slides using a Leica CM3050 cryostat. Slides were dried and stored at -20°C.

Live-cell imaging

Live-cell imaging was performed using spinning disk confocal microscopy, using an Olympus IX70 microscope with a Hamamatsu EM-CCD Image-EM camera and a PerkinElmer Ultra-VIEW scanner. Videos were taken using Meta-Morph software. Rab11 and integrin vesicle trafficking along the axon was imaged at the proximal (up to 100μm) and distal part (beyond 600μm) of axons of neurons transfected with Protrudin (as described before in 9,10). One image per second was obtained for 3 minutes. Kymographs were obtained by measuring an individual axon segment. Anterograde, retrograde, bidirectional and static modes of transport were measured. The percentage of co-localization between integrin or rab11 and Protrudin was calculated as the number of vesicles containing either was divided by the total number of vesicles. All analysis was performed using Meta-Morph software.

Western Blotting

PC12 cells were transfected using lipofectamine. 48 hours later cells were lysed using the cOmplete Lysis Kit (Roche). Cells were washed with ice-cold PBS. 500 μL of pre-cooled lysis buffer was added to each well of a 6-well plate and the lysate was scraped using a cell scraper and

bioRxiv preprint doi: https://doi.org/10.1101/2020.01.15.907550; this version posted January 15, 2020. The copyright holder for this preprint (which was not certified by peer review) is the author/funder. All rights reserved. No reuse allowed without permission.

transferred to a sterile 1.5 mL Eppendorf. The lysate was incubated on ice for 30 minutes with occasional mixing. The samples were then centrifuged at 10 000 g at 4°C for 10 minutes. The supernatant was transferred to 1.5 mL Eppendorf and the pellet was discarded. The total protein concentration was measure by BCA assay using Pierce BCA Assay Kit Protocol (ThermoFischer Scientific). The 96-well plate containing the sample lysates and BCA reagents was analyzed using Gen5.1 software and concentrations were derived from a standard curve for albumin control. 15 µg of PC12 cell lysate was then treated with LDS Sample Buffer NuPAGE 4x (1:4, ThermoFisher Scientific) and Sample Reducing Agent (1:10, ThermoFisher Scientific) and were analyzed by Western blot. Samples were run on a 4-12% gel at 120 V at room temperature in 40 mL Running Buffer NuPAGE (ThermoFisher Scientific) diluted in H20 to 800 mL. The gel was then transferred onto a nitrocellulose membrane (Invitrolon PDVF/Filter Paper Sandwich, ThermoFischer Scientific) for 1.5 hours at 40V at 4°C in 50 mL Transfer Buffer NuPAGE (ThermoFisher Scientific) in 100 mL methanol, topped up with ddH20 to 1 L. The membrane was then blocked either in 5% milk or 3% BSA depending on the antibody for 1 hour and incubated overnight with the primary antibody diluted the blocking solution to the right concentration at 4°C. The membrane was then rinsed three times in Tris-buffered saline with Tween 20 (TBST buffer) for 10 minutes each. The TBST buffer was removed. Secondary peroxidase-conjugated antibodies were diluted to the right concentration in blocking solution and were then added for 1 hour at room temperature. SuperSignal West Dura Extended Duration Substrate kit (ThermoFischer Scientific) and Alliance software were then used for detection.

Axotomy

10DIV neurons were transfected with various constructs using magnetofection as described above. Between 13-17 DIV, their regeneration ability was examined using the laser axotomy model described in detail in (4). Axotomy was performed by an UV Laser (355 nm, DPSL-355/14, Rapp OptoElectronic, Germany) connected to a Leica DMI6000B (Leica Systems, Germany), and all images were taken with an EMCCD camera (C9100-02, Hamamatsu). Axons were cut at least 600 µm away from the cell body and regeneration was observed for 14 hours post injury at 30-minute intervals. If more than 50% neuronal cell death occurred in the axotomised cells, the experiment was excluded from the final analysis.

bioRxiv preprint doi: https://doi.org/10.1101/2020.01.15.907550; this version posted January 15, 2020. The copyright holder for this preprint (which was not certified by peer review) is the author/funder. All rights reserved. No reuse allowed without permission.

Animal Studies

All procedures were performed in accordance with protocols approved by the Institutional Animal Care and Use Committee (IACUC) at the National Institutes of Health. Female C57Bl/6 mice aged 6-8 weeks (Charles River) (n=27) were housed in a pathogen-free facility with free access to food and a standard 12 h light/dark cycle. Intravitreal injections of viruses were administered 14 days prior to optic nerve crush or whole retinal explant. 5 μL of the injecting solution for mice was drawn into a sterile 5 μL Hamilton syringe equipped with a 33-gauge removable needle. The solution was injected into the vitreous humor through the superior nasal sclera, with the needle positioned at a 45° angle to avoid the lens, external ocular muscle, and blood vessels. Before removing the needle, a sterile 33-gauge needle was used to puncture the cornea and drain the anterior chamber, thereby reducing intraocular pressure and preventing reflux. Different needles were used for each virus to prevent contamination, and syringes were rinsed between injections with ethanol followed by sterile PBS.

Optic Nerve Crush

Optic nerve crush was performed as described (28). Micro-scissors were used to make an incision in the conjunctiva and expose the optic nerve. Curved forceps were then inserted below the external ocular muscle, avoiding the ophthalmic artery and retrobulbar sinus, and positioned around the exposed nerve. The nerve was crushed for 10 s approximately 1 mm behind the eye. Following the crush, eyes were observed fundoscopically for signs of ischemia, and mice were monitored for signs of intraorbital bleeding. Mice were given a subcutaneous injection of 1 mg/kg buprenorphrine as an analgesic and topical application of ophthalmic ointment to prevent corneal drying. Intravitreal injections of CTB (1.0 μg/μL, Sigma) were administered 2 d prior to perfusion. 2 μL of the solution injected as described above.

Whole retina explant culture

Mice were euthanized by cervical dislocation, eyes enucleated, and placed immediately into ice-cold HBSS. Retinas were dissected from the eyes in HBSS on ice, flat-mounted with the ganglion cell layer up on a cell culture insert (Millipore), and submerged in tissue culture media containing Neurobasal –A, 1% penicillin-streptomycin (10000 U/ml), 1% glutamine (100X), 1% N-2 (100X)

bioRxiv preprint doi: https://doi.org/10.1101/2020.01.15.907550; this version posted January 15, 2020. The copyright holder for this preprint (which was not certified by peer review) is the author/funder. All rights reserved. No reuse allowed without permission.

and 1% B-27 (50X) (all ThermoFisher Scientific). Retinas were incubated in 6-well plates at 37 °C and 4% CO_2 for 3 days and were fed by replacing 50% of the media on day 2. Retina were fixed in 3.7% PFA and stained with antibodies against RBMPS and GFP followed by counterstaining with DAPI. For untreated "DEV 0" controls, retinas were dissected and placed straight into 3.7% PFA.

Statistics

Statistical analysis was performed using GraphPad Prism 8.0 (GraphPad Software, La Jolla, CA). Each data set was individually tested for normal distribution using the D'Agostino-Pearson normality test. When data was normally distributed one-way ANOVA with multiple comparisons was used to test statistical significance between the experimental groups with Tukey's post hoc test. Several data sets were shown to be non-normally distributed. Therefore, a non-parametric Kruskal-Wallis test with multiple comparisons was used to test for significant differences across experimental groups. Dunn's multiple comparison post-hoc test was also performed. All statistics were carried out at 95% confidence intervals, therefore a significant threshold of $p<0.05$ was used in all analyses. For Sholl analysis, repeated measures two-way ANOVA was performed using SPSS (IBM Statistics). When comparing percentages (e.g. of regenerating cells), Fisher's exact test was performed between each two groups compared. p-values were then analyzed with the "Analyze a stack of p values" function in GraphPad Prism with a Bonferroni-Dunn pairwise comparison to test for statistical significance between groups.

bioRxiv preprint doi: https://doi.org/10.1101/2020.01.15.907550; this version posted January 15, 2020. The copyright holder for this preprint (which was not certified by peer review) is the author/funder. All rights reserved. No reuse allowed without permission.

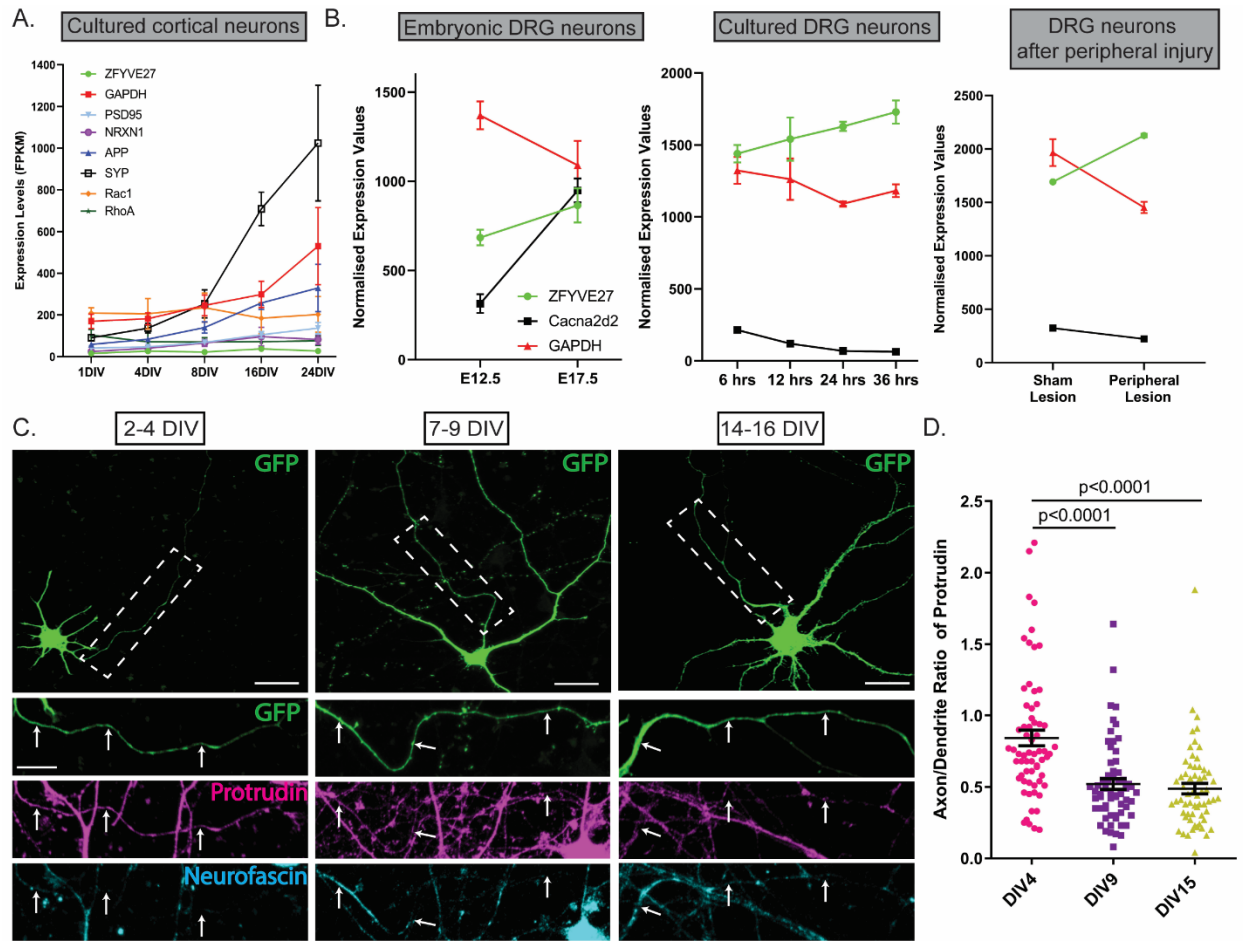

Figure S1 Protrudin is expressed at low levels in the CNS and has a somatodendritic localization in mature neurons. (**A**) mRNA expression levels of six neuronal genes (including *Zfyve27* – the Protrudin gene) from different stages of development in primary rat cortical neurons *in vitro*. (**B**) Normalized expression levels of Protrudin and other related genes during embryonic development in the mouse, after plating DRG neurons *in vitro* or after peripheral nerve injury in DRG cells. (**C**) Immunofluorescent images of Protrudin in the proximal axons (white dotted line box) of neurons at different stages of development in culture. Scale bars are 20 µm. The white arrows follow the course of the proximal axon. (**D**) The axon-to-dendrite ratio of Protrudin at different developmental stages ($n = 4$, *Kruskal-Wallis with Dunn's* multiple comparison test, $p < 0.0001$). Error bars represent mean ± SEM.

bioRxiv preprint doi: https://doi.org/10.1101/2020.01.15.907550; this version posted January 15, 2020. The copyright holder for this preprint (which was not certified by peer review) is the author/funder. All rights reserved. No reuse allowed without permission.

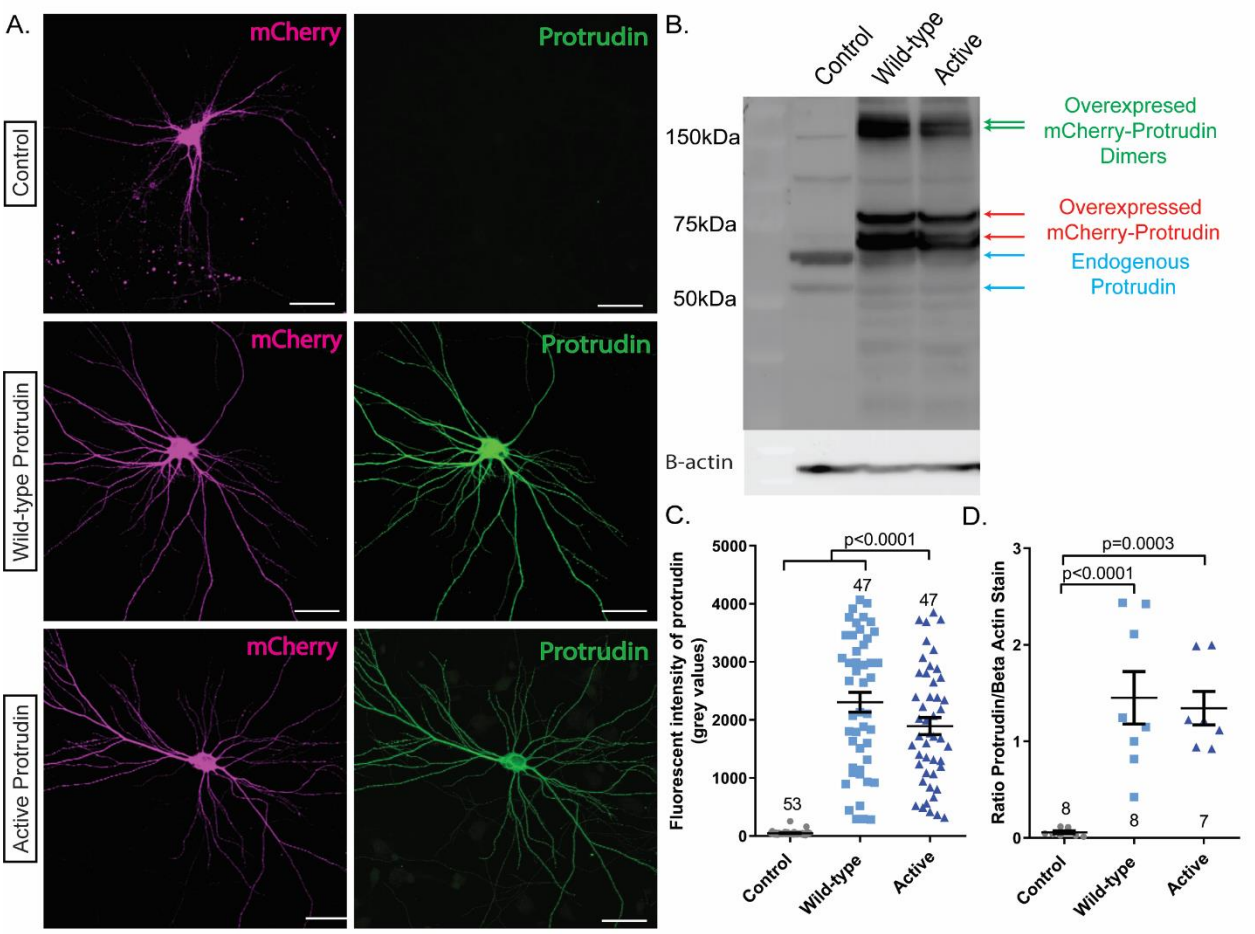

<u>Figure S2</u> Overexpression of Protrudin results in higher amount of the Protrudin protein in rat cortical neurons at 14 DIV. (**A**) Images showing mCherry fluorescence (magenta) and Protrudin immunofluorescence (green) from neurons transfected with syn-mCh control (Control), syn-mCh-WT (wild-type Protrudin) or syn-mCh-active (active Protrudin) (magenta) and labelled with anti-Protrudin antibody. Scale bars are 20 µm. (**B**) Western blot showing Protrudin expression levels in PC12 cells overexpressing the three different constructs. The blot was stripped and probed for beta actin (lower panels). Blue arrows indicate endogenous Protrudin, red arrows indicate overexpressed Protrudin-mCherry and green arrows show overexpressed mCherry-tagged Protrudin dimers. (**C**) Scatter plot to show the average fluorescence intensity of Protrudin in transfected neurons (n = 3, *Kruskal-Wallis with Dunn's* multiple comparison test, $p < 0.0001$). (**D**) Scatter plot to show the ratio of protrudin to beta actin staining of PC12 lysate extracted from cells overexpression either control, wild-type protrudin or active protrudin constructs (n = 7-8, *Kruskal-Wallis with Dunn's* multiple comparison test, $p < 0.0001$). Error bars represent mean ± SEM.

bioRxiv preprint doi: https://doi.org/10.1101/2020.01.15.907550; this version posted January 15, 2020. The copyright holder for this preprint (which was not certified by peer review) is the author/funder. All rights reserved. No reuse allowed without permission.

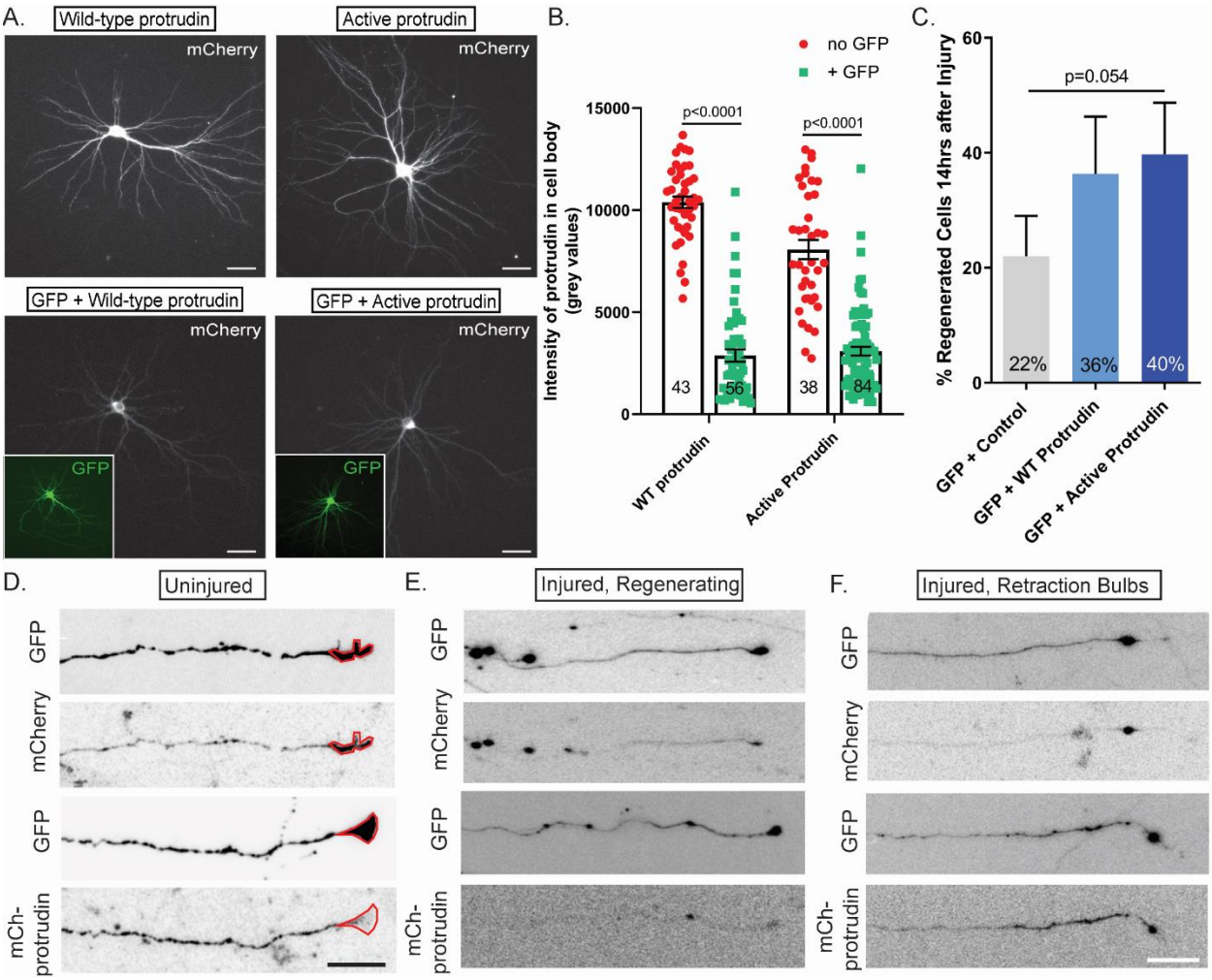

<u>Figure S3</u> Protrudin promotes regeneration in a dose-dependent manner and localizes to the axon tip. (**A**) Immunofluorescence images of cells expressing wild-type or active Protrudin on their own or in combination with GFP control plasmid. Scale bars are 20 µm. (**B**) Quantification of mCherry-Protrudin fluorescence intensity in the soma. (**C**) Percentage of regenerating axons after laser axotomy in neurons co-transfected with Protrudin constructs and GFP. (**D**) Representative images showing GFP and mCherry-Protrudin at the growth cone of neurons co-expressing both constructs. Red lines indicate the area of the growth cone as defined by the GFP signal. Scale bars are 10 µm. (**E**) Images showing regenerating axons after injury. Scale bars are 20 µm. (**F**) Images showing retraction bulbs of non-regenerating processes after laser axotomy. Scale bars are 20 µm.

bioRxiv preprint doi: https://doi.org/10.1101/2020.01.15.907550; this version posted January 15, 2020. The copyright holder for this preprint (which was not certified by peer review) is the author/funder. All rights reserved. No reuse allowed without permission.

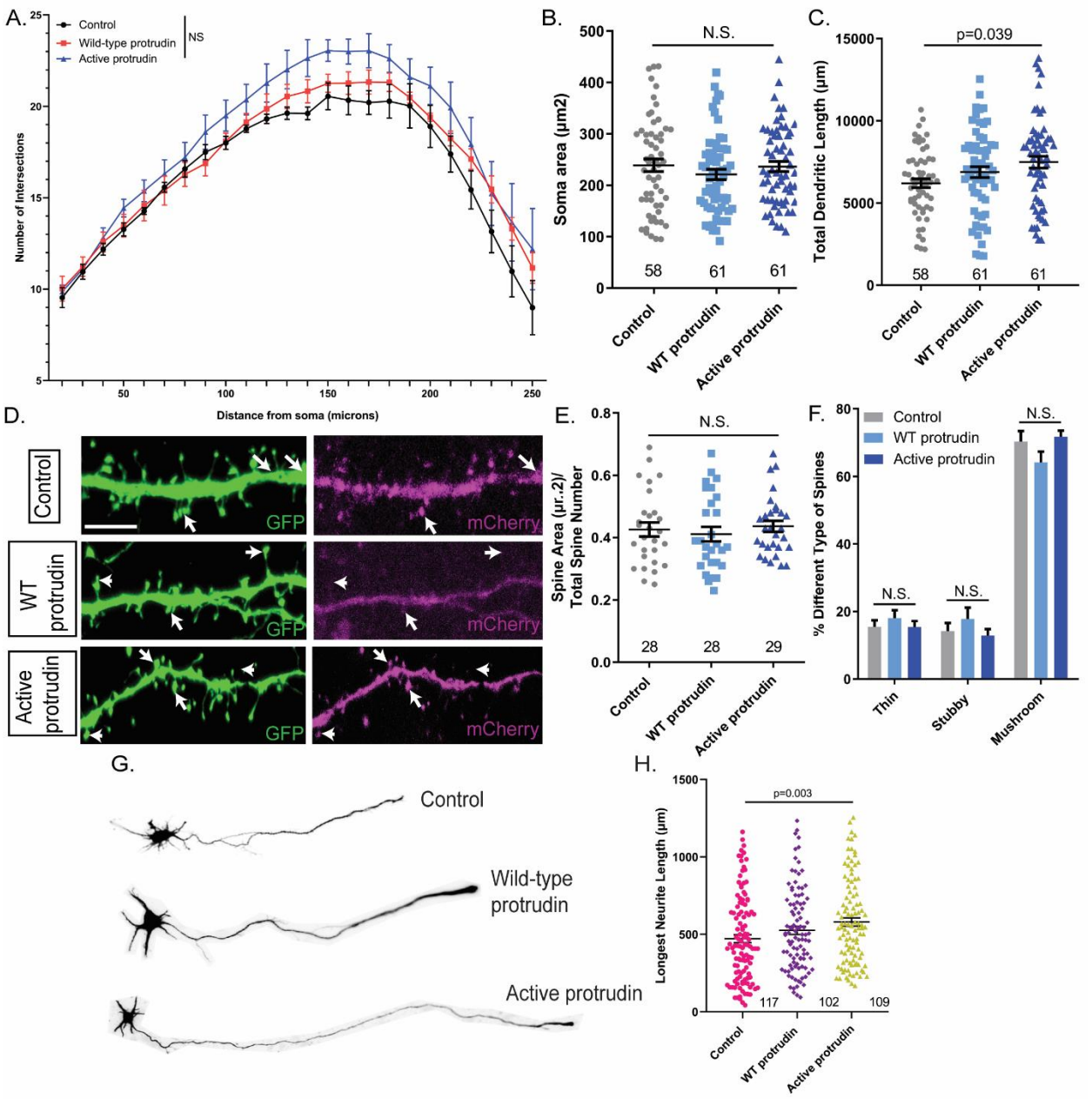

<u>Figure S4</u> Overexpression of Protrudin does not result in morphological changes and active Protrudin has a modest effect on neurite length. (**A**) Dendritic tree complexity of neurons transfected with each construct - the number of intersections at each distance from the cell soma was plotted for each condition. There are no significant differences between the conditions (n = 4, repeated measures *2-way ANOVA*). (**B**) Average soma area in cells expressing the three different mCherry constructs (n = 5, p = 0.142, *Kruskal-Wallis with Dunn's* multiple comparison test). (**C**) Dendritic tree total length across the different conditions. Cells overexpressing active Protrudin

bioRxiv preprint doi: https://doi.org/10.1101/2020.01.15.907550; this version posted January 15, 2020. The copyright holder for this preprint (which was not certified by peer review) is the author/funder. All rights reserved. No reuse allowed without permission.

have a more complex dendritic structure than cells overexpressing control (n = 4, p = 0.067, *one-way ANOVA*). (**D**) Representative z-project images of 20 μm z-stack sections examined for dendritic spine number and morphology. White arrows point to individual spines. Scale bars are 5 μm. (**E**) The spine area (μm^2) per the total number of spines for each condition. There were no significant differences between the four conditions (n = 2, p = 0.127, *Kruskal-Wallis with Dunn's* multiple comparison test). (**F**) There are no changes in spine morphology between the different conditions. (**G**) Example neurons at 4 DIV overexpressing control construct, wild-type or active Protrudin. (**H**) The average length of the longest neurite in each condition (n = 3, p = 0.01, *Kruskal-Wallis with Dunn's* multiple comparison test). Error bars represent mean ± SEM.

bioRxiv preprint doi: https://doi.org/10.1101/2020.01.15.907550; this version posted January 15, 2020. The copyright holder for this preprint (which was not certified by peer review) is the author/funder. All rights reserved. No reuse allowed without permission.

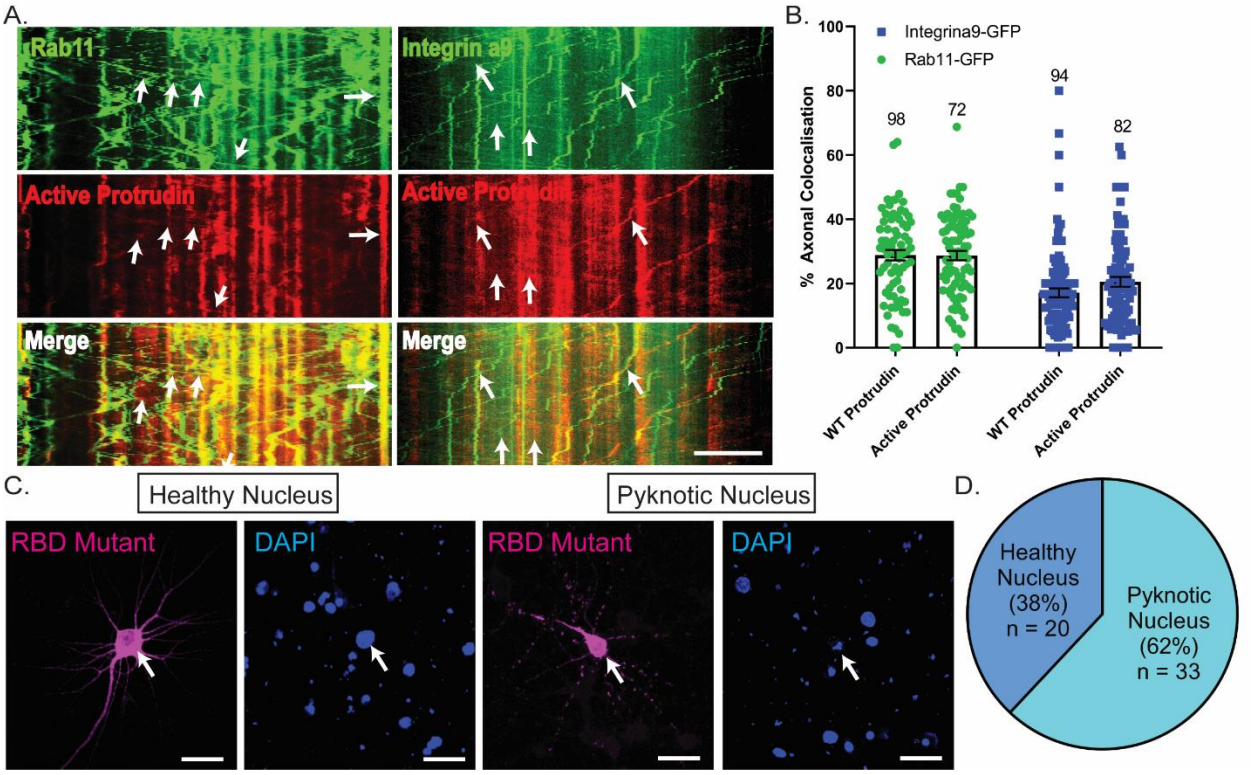

<u>Figure S5</u> Rab11 and integrin vesicles co-localize with Protrudin and RBD domain deletion has consequences on cell survival. (**A**) Kymographs showing co-localization between Rab11 or integrin α9-GFP with Protrudin. (**B**) Wild-type and active Protrudin co-localize to similar extent with either Rab1 or integrin alpha 9. Error bars represent mean ± SEM. (**C**) Representative fluorescent images of RBD mutant of Protrudin in surviving and non-surviving (the most common phenotype) cells as shown by nuclear fragmentation (pyknosis). Scale bars are 20 µm. (**D**) Pie chart showing the percentage of cells with healthy and pyknotic nuclei in cortical neurons overexpressing RBD mutant protrudin (n=3).

bioRxiv preprint doi: https://doi.org/10.1101/2020.01.15.907550; this version posted January 15, 2020. The copyright holder for this preprint (which was not certified by peer review) is the author/funder. All rights reserved. No reuse allowed without permission.

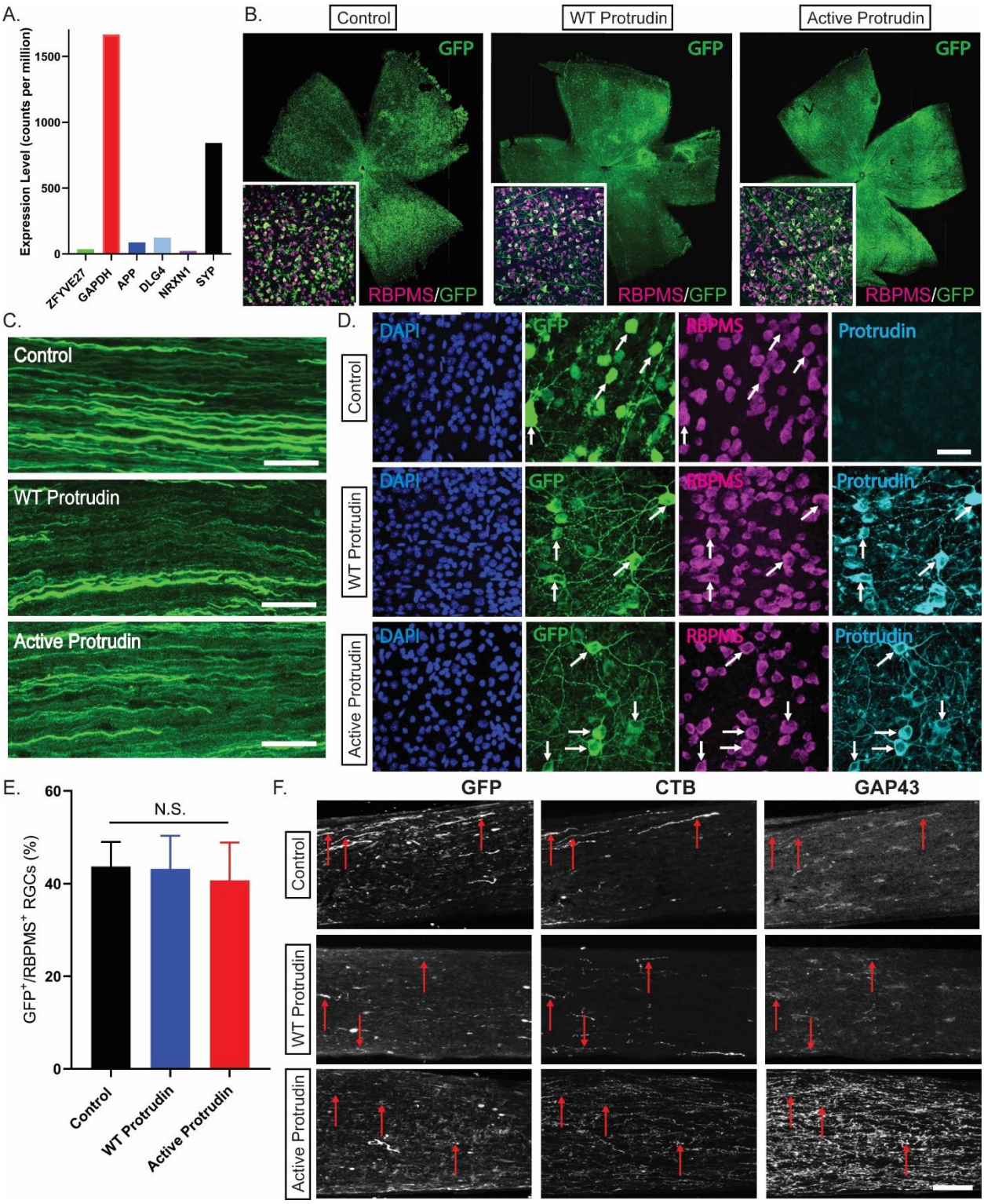

<u>Figure S6</u> Protrudin viruses are expressed in RGCs throughout the retina and the optic nerve and regenerating axons are GAP43 and CTB positive. (**A**) Protrudin mRNA levels during the

bioRxiv preprint doi: https://doi.org/10.1101/2020.01.15.907550; this version posted January 15, 2020. The copyright holder for this preprint (which was not certified by peer review) is the author/funder. All rights reserved. No reuse allowed without permission.

progression of glaucoma in comparison to other neuronal markers. (**B**) Retinal wholemounts or axonal sections showing GFP-positive cells which have been transduced with one of three viruses: control GFP, wild-type Protrudin or active Protrudin-GFP. Retinas were immunostained for RBPMS - retinal ganglion cell marker (magenta) showing co-localization between the virally infected cells (GFP) and RGCs. (**C**) Viral expression is detected in RGC axons. Scale bar is 20 µm. (**D**) Retinal sections showing co-localization between RBPMS (magenta) and GFP (green) and elevated Protrudin levels (cyan) as detected by immunohistochemistry. Scale bars are 20 µm. (**E**) Robust viral expression in RGC-positive cells was detected for all constructs (n = 2 per condition). (**F**) Immunolabelled optic nerve sections for GAP-43, CTB and GFP. Red arrows show regenerating axons where GFP, CTB and GAP43 all co-localize. Scale bars are 10 µm.